Kinetics, Products, and Brown Carbon Formation by Aqueous-Phase Reactions of Glycolaldehyde with Atmospheric Amines and Ammonium Sulfate

*Alyssa A. Rodriguez,[1]Michael A. Rafla,[1] Hannah G. Welsh,[2] Elyse A. Pennington,[2] Jason R. Casar,[2] Lelia N. Hawkins,[2] Natalie G. Jimenez,[1] Alexia de Loera,[1] Devoun R. Stewart,[1†] Antonio Rojas,[1] Matthew-Khoa Tran,[1] Peng Lin,[3††] Alexander Laskin,[3] Paola Formenti,[4] Mathieu Cazaunau,[4] Edouard Pangui,[4] Jean-François Doussin,[4] David O. De Haan[1]**

[1] Department of Chemistry and Biochemistry, University of San Diego, 5998 Alcala Park, San Diego CA 92110 USA

[2] Department of Chemistry, Harvey Mudd College, 301 Platt Blvd, Claremont CA 91711 USA

[3] Environmental Molecular Sciences Laboratory, Pacific Northwest National Laboratory, Richland, Washington 99352, USA, and Department of Chemistry, Purdue University, West Lafayette IN 47907 USA

[4] Laboratoire Interuniversitaire des Systèmes Atmosphériques (LISA), UMR7583, CNRS, Université Paris-Est Créteil (UPEC) et Université de Paris, Institut Pierre Simon Laplace (IPSL), 94000 Créteil, France

†: now at Department of Chemistry, Sacramento City College, 3835 Freeport Blvd. Sacramento, CA 95822 USA

††: now at California Air Resources Board, 4001 Iowa Ave., Riverside, CA, 92507 USA

* Corresponding author contact: 011-1-619-260-6882, -011-1-619-260-2211 fax, ddehaan@sandiego.edu

Keywords: secondary organic aerosol, aldehydes, cloud chemistry, aldol condensation, Maillard reactions, complex index of refraction

ABSTRACT: Glycolaldehyde (GAld) is a C_2 water-soluble aldehyde produced during the atmospheric oxidation of isoprene and many other species, and is commonly found in cloud water. Previous work has established that glycolaldehyde evaporates more readily from drying aerosol droplets containing ammonium sulfate (AS) than does glyoxal, methylglyoxal, or hydroxyacetone, which implies that it does not oligomerize as quickly as these other species. Here, we report NMR measurements of glycolaldehyde's aqueous-phase reactions with AS, methylamine and glycine. Reaction rate constants are smaller than those of respective glyoxal and methylglyoxal reactions in the pH range 3 - 6. In follow-up cloud chamber experiments, deliquesced glycine and AS seed particles were found to take up glycolaldehyde and methylamine and form brown carbon. At very high relative humidity, these changes were more than two orders of magnitude faster than predicted by our bulk liquid NMR kinetics measurements, suggesting that reactions involving surface-active species at crowded air-water interfaces may play an important role. High-resolution liquid chromatography-electrospray ionization-mass spectrometric analysis of filter extracts of unprocessed AS+GAld seed particles identified sugar-like C_6 and C_{12} GAld oligomers, including proposed product *3*-deoxyglucosone, with and without modification by reactions with ammonia into diimine and imidazole forms. Chamber exposure to methylamine gas, cloud processing, and simulated sunlight increased the incorporation of both ammonia and methylamine into oligomers. Many C_4 – C_{16} imidazole derivatives were detected in an extract of chamber-exposed aerosol, along with a predominance of *N*-derivatized C_6 and C_{12} glycolaldehyde oligomers, suggesting that GAld is capable of forming brown carbon SOA.

1. Introduction

Glycolaldehyde (GAld) is a small, highly water-soluble molecule produced by the oxidation of many atmospheric precursors, including isoprene.[1] Its global production rate from isoprene + ·OH

oxidation has been estimated at 42 Tg C yr^{-1}.[2] In the gas phase, GAld reacts with photochemical oxidants to produce glyoxal and smaller species,[3, 4] with a midday lifetime of several hours.[1, 5] Like other small aldehydes, GAld is routinely detected in aqueous aerosol and cloudwater,[6-9] even in remote areas, due to its ability to react with water to form a hydrate. Aqueous phase photooxidation of GAld is a significant source of aqueous secondary organic aerosol (aqSOA),[10] since its reaction with dissolved OH radicals produces glyoxal, glycolic, oxalic, malonic, and succinic acids, larger oligomers,[2] and organosulfate species.[11] Additionally, GAld reacts in Maillard-type aqueous reactions with ammonium sulfate (AS)[12-14] and amines (especially glycine)[13] to form visible-light-absorbing products known as brown carbon (BrC) and also N-containing heterocyclic oligomers such as imidazoles and pyrazines.[14] However, in laboratory studies where airborne droplets containing AS or amines were dried for several minutes with and without dissolved GAld, the presence of GAld slowed down the evaporation process, but did not measurably increase the size of the dried residual particles (except for 1:2 glycine:GAld mixtures).[15, 16] For this reason, it is not yet clear the extent to which Maillard dark reactions involving GAld can contribute to aqSOA or BrC production in atmospheric cloud droplets and aqueous aerosol.

In this study, we determine pH-dependent GAld+AS, GAld+glycine, and GAld+methylamine dark reaction kinetics using nuclear magnetic resonance (NMR) measurements of reactant loss rates in D_2O solutions. Additionally, in large chamber experiments we characterize SOA and BrC formation from GAld+glycine and GAld+AS+methylamine reactions as a function of relative humidity (RH). We identify sugar-like and N-containing aqueous-phase products formed after GAld uptake into aqueous aerosol particles containing AS, with and without cloud processing. We find that exposure of GAld+AS aerosol to methylamine gas and dark and sunlit cloud processing increases incorporation of both methylamine and ammonia into C_6 and C_{12} GAld oligomers.

2. Materials and Methods

2.1. Chemicals and pH.

All chemicals were purchased from Sigma-Aldrich unless otherwise stated. Stock solutions were made by overnight hydrolysis of GAld dimer, dilution of 40% aqueous solutions of methylamine (Spectrum), or dissolution of solid glycine or ammonium sulfate (AS), all in D_2O (99.9%-D, Cambridge Isotopes) for NMR experiments or in 18MΩ deionized water for chamber experiments. Amine or AS samples in D_2O were pH-adjusted using acetic acid-*d6* or sodium phosphate.

2.2. NMR data processing and derivation of rate constants

For reaction rate constant measurements, stock solutions in D_2O with 1% v/v acetonitrile (an internal standard at 2.061 ppm) were vortex mixed in an NMR tube to reach initial concentrations of 0.5 M for each reactant at $t = 0$. Reaction mixture pH was measured immediately after mixing replicate samples in vials. Proton NMR spectra were recorded continuously (Varian, 400 or 500 MHz) over at least 16 h at room temperature. Table 1 lists the chemical shifts and locations of H atoms used for NMR quantitation of reactant compounds. After phasing and baseline correction, integrated ^1H peak areas were normalized by acetonitrile. GAld monomer NMR signals increased by ~10% in the first hour after mixing due to an equilibrium shift from dimer to monomer in response to a factor-of-two dilution caused by the mixing of the reactant solutions. Once GAld monomer-dimer equilibrium is achieved, declines in GAld NMR signals caused by other chemical reactions can be measured. Because GAld dimer hydrolysis has a half-life of ~2 h,[17] initial reaction rates were extracted from each NMR signal listed in Table 1 starting at $t = 3$ h. Normalized initial amine and aldehyde peak areas at $t = 3$ h were set equal to nominal concentrations of each reactant.

Very slow reaction rates with rate constants < 2×10^{-5} M^{-1} s^{-1} could not be detected by NMR measurements of reactant loss.

Table 1: NMR signals used for quantitation of reactants

Reactant molecule	functional group	NMR chemical shift (ppm)
hydrated glycolaldehyde monomer	CH_2	3.50
hydrated glycolaldehyde monomer	CH	5.05
methylamine	CH_3	2.58
glycine	CH_2	3.55

The reaction order in this work was assumed to be first order in GAld and first order in amine or AS, like other Maillard reactions at low-to-moderate concentrations.[18-23] Rate constants are given for active (aldehyde) forms of GAld, rather than total GAld (aldehyde + hydrate forms). The second-order rate constant is derived from the measured initial reaction rate using the following equation:[24]

$$Rate = k\, f_{Ald}\, [Ald]_{tot}\, [Am]_{tot} \quad (1)$$

where *Rate* represents a measured initial reactant rate, k is the second-order rate constant in M^{-1} s^{-1}; $[Ald]_{tot}$ and $[Am]_{tot}$ are the total concentrations in M of hydrated and unhydrated GAld and protonated and unprotonated amine (or ammonium), respectively; and f_{ald} is the equilibrium fraction of GAld in aldehyde (not hydrate) form, determined to be $f_{ald} = 0.053$ at room temperature by computational[17] and NMR methods.[17, 25] We do not calculate pH-independent rate constants based on concentrations of deprotonated ammonia and amines because, as shown below, rates were not directly proportional to concentrations of the deprotonated species.

2.3. Chamber experiments and ESI-HRMS analysis

Cloud processing experiments took place in the 4.2 m^2 CESAM chamber.[26, 27] Experimental start times were defined as the beginning of N_2 and O_2 addition to the evacuated chamber. Seed aerosol particles were generated from 1.8 mM AS, 2.0 mM glycine, or a mixture containing 1.8 mM AS

and 50 mM GAld. Mixed AS+GAld aerosol were also collected directly on a filter without chamber exposure as a control. In three experiments in the chamber, seed aerosols were exposed to various combinations of gas-phase GAld, methylamine, 1-2 cloud events of 5-10 min. duration each, and/or 60-75 min. of simulated sunlight. Cloud events (supersaturation) were triggered by a combination of expansion-cooled water vapor injection and a gradual, 10% pressure reduction. The evolution of cloud droplet size distributions was characterized from a chamber flange by optical scattering (Palas Welas Digital 2000, 0.5 to 15 μm range).[26] Experimental conditions are summarized in Table 2. Gas-phase species were monitored by PTR-MS (KORE Tech. Series II) and sensors for RH, NOx, NO, NO_2, and ozone. PTR-MS signals for GAld at *m/z* 61 contain a significant contribution from the contaminant molecule acetic acid, which was detected whenever water vapor was added to the chamber. However, GAld and acetic acid contributions to *m/z* 61 signals were deconvoluted using *m/z* 43, since the two compounds have very different *m/z* 61 / 43 ratios, as shown in Figures S1 and S2.

Table 2: Summary of chamber experiments involving glycolaldehyde

expt	aerosol seed	$[GAld]_g$ (ppm)	$[MeAm]_g$ (ppm)	sun	clouds (#)	filter collected	figures
1	Glycine	1	0	no	1	no	3, S1, S3
2	AS/GAld	0	1	yes	2	yes	4, S2, S4
3[a]	AS/GAld	0	0	no	0	yes	
4	AS	0.3	1	yes	2	no	S5

a: Control experiment: seed particles were collected directly on filter without any exposure to methylamine gas, simulated sunlight, or cloud events in chamber.

Aerosol physical and optical properties were monitored by scanning mobility particle sizing (SMPS, TSI), particle-into-liquid sampling (PILS)-waveguide UV-vis absorbance spectroscopy (1 m pathlength), and cavity attenuated phase shift single-scattering albedo (CAPS-ssa, Aerodyne, 450 nm) spectroscopy.[28] SMPS and CAPS-ssa data, both collected after drying aerosol through a Nafion sampling tube, were used to back-calculate time-dependent complex indices of refraction

using an IDL routine over a 2-D range of n (1.33 to 2.00, step 0.01) and k values (0 to 0.050, step 0.001). Shape factors (1 to 1.1, step 0.02) were tested, but no evidence of non-sphericity (shape factors > 1.00) was found. All n and k combinations that produced extinction and scattering values that matched observations within the measurement uncertainty were retained, then averaged to produce the reported n and k values. Since aerosol-phase total organic carbon was not quantified, PILS-waveguide data was converted to mass absorption coefficients (MAC) in this study only in experiments where aerosol growth was observed (expt. 2) or where seed particles contained glycine (expt. 1), since in these cases we could estimate total organic carbon in the aerosol. TOC estimates and MAC calculations are described in the Supplemental Information.

After chamber processing concluded, aerosol samples were collected at 15 L/min onto Teflon filters over 16 h while the chamber pressure was held constant with a compensating dry N_2 inlet flow. Chamber and control filters were frozen at -20°C until extraction by acetonitrile immediately prior to ESI-HRMS analysis (Surveyor Plus system with HPLC pump, autosampler and PDA detector, IonMAX electrospray ionization (ESI) source, and high resolution LTQ-Orbitrap mass spectrometer, Thermo Electron).[29] The details of the ESI-HRMS experimental setup, data acquisition, peak deconvolution, and molecular formula assignment have been described previously.[30] We report exact masses of all peaks detected with areas greater than 10^6 and elevated relative to blank extract runs. No unusual safety hazards were encountered during the course of this work.

3. Results

3.1. Bulk aqueous phase glycolaldehyde reaction kinetics.

A summary of second-order rate constants derived from NMR measurements of reactant loss rates in D_2O is shown in Figure 1. These rate constants were calculated using total (protonated +

unprotonated) concentrations of ammonia or amines present. Rate constants for all three reactions (glycolaldehyde + methylamine, glycine, or AS) were smaller than those measured for respective glyoxal or methylglyoxal reactions,[24] but showed a significant pH dependence, as expected for Maillard-type chemistry. If reaction rates were proportional to concentrations of unprotonated ammonia or amine species, the least squares fits in Figure 1 would have slopes = 1 (shown as a gray dotted line in each panel for comparison). Instead, pH dependence is substantially less than that (*i.e.* a slope of one is outside the $\pm 3\sigma$ range of the least square fits). Furthermore, if reaction rates were solely a function of deprotonated nitrogen atom concentrations, GAld+AS rate constants would be the highest at all pH, because ammonia is a weaker base than either amine species, and so a greater fraction remains unprotonated. For GAld reactions with AS and glycine, rates appear to depend more strongly on pH above pH ~5. Below pH 5, pH dependence appears to flatten, and GAld loss rates converge for all three reaction mixtures. Finally, in GAld+methylamine mixtures (blue symbols) with pH < 7, loss rates of methylamine are substantially less than those of GAld.

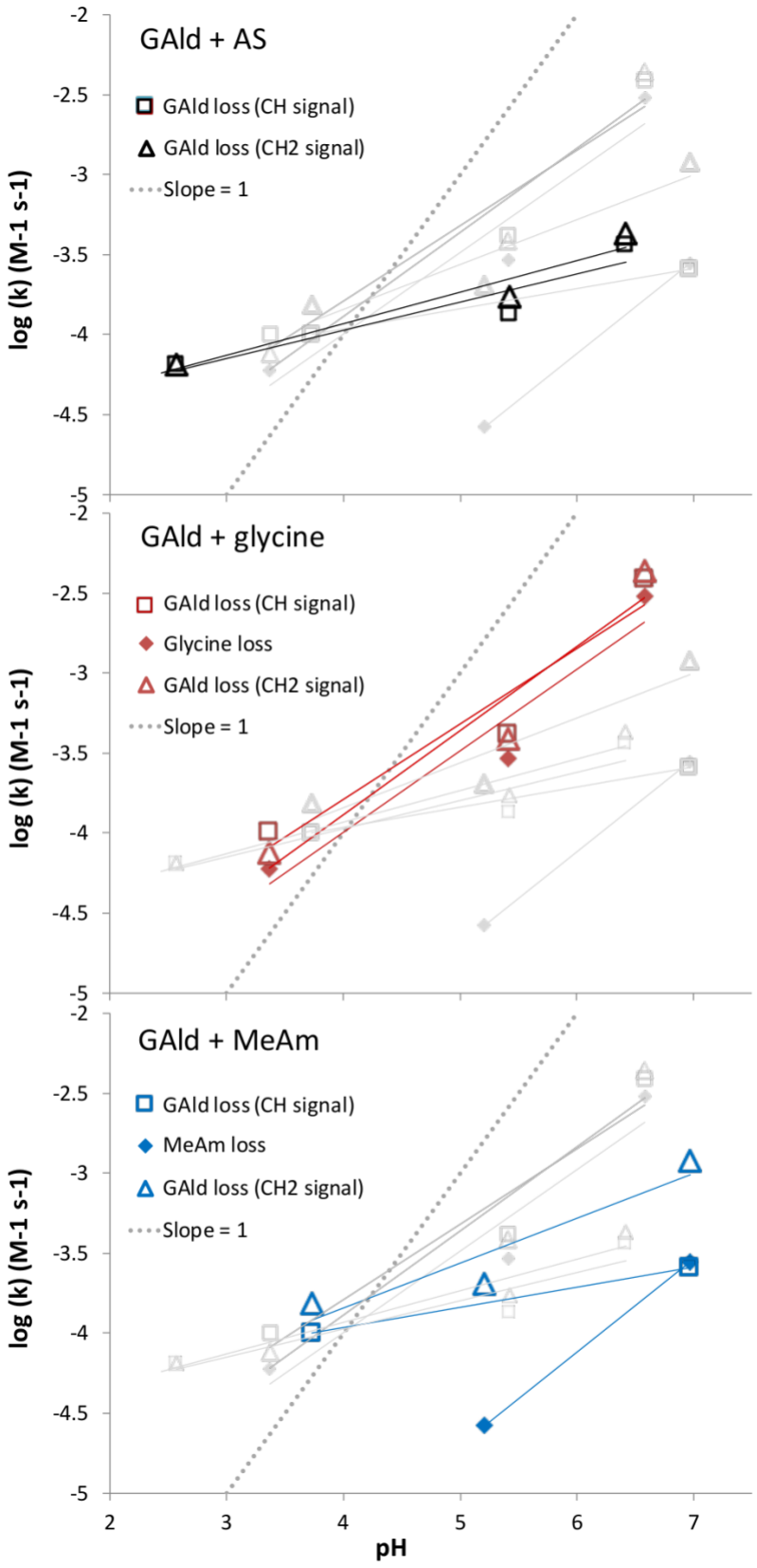

Figure 1: Apparent second-order rate constants ($M^{-1}s^{-1}$) measured by ^{1}H-NMR for bulk aqueous phase glycolaldehyde reactions at room temperature. Identical data is shown in each panel, along with a slope = 1 dotted line for comparison. Individual panels highlight reactions with AS (in black, top), glycine (red, middle), and methylamine (blue, bottom); initial concentrations = 0.5 M. Rate constants are calculated from losses of reactant signals: glycolaldehyde losses were followed at the CH_2 signal (3.50 ppm, open triangles) and the CH signal (attached to the hydrated carbonyl, 5.05 ppm, open squares). Amine losses (filled diamonds) were calculated from methylamine CH_3 (2.58 ppm) and glycine CH_2 (3.55 ppm) signals. AS losses could not be measured, and

202 methylamine losses at pH 3.7 were below the method detection limit.

These observations suggest that more than one reaction mechanism is in operation across the pH 2 – 7 range. At near-neutral pH, the reaction between reduced nitrogen and the carbonyl functional group appears to be the main sink for both compounds, causing a steeper pH dependence. At lower pH, an acid-catalyzed GAld self-reaction appears to be the dominant sink, consistent with the similar GAld loss rates observed at low pH in all three reaction mixtures. GAld aldol self-reactions are also catalyzed by ammonium and aminium ions,[20, 23, 31] which may explain why methylamine loss rates are far less than GAld loss rates below pH 7. For the GAld+glycine reaction, the ratio of glycolaldehyde to glycine loss rates stayed constant across the pH range at 1.41 (±0.07) to 1, in contrast to the GAld+MeAm reaction. This indicates both a non-negligible role of GAld self-reactions even at neutral pH, and some level of glycine reactivity even under acidic conditions. Interestingly, GAld+glycine mixtures have been shown to brown much more efficiently than GAld+MeAm or GAld+AS mixtures at pH 4.[15] This difference must be due to formation of products with higher molar absorptivities in the GAld+glycine system, since the GAld loss rate kinetics are similar for all 3 systems at this pH.

By making an initial assumption that these pH-dependent rate constants measured for the loss of GAld CH_2 groups in bulk liquid with glycine and methylamine are applicable to reactions with all amino acids and other primary amines, respectively, in suspended aqueous aerosol and cloud droplets, we can estimate the relative size of various atmospheric sinks for aqueous-phase glycolaldehyde. For this estimation we used typical cloudwater concentrations of radical species ([OH radical] = 1×10^{-13} M),[32] amine aqueous aerosol concentrations enriched by a factor of 10^4 over measured concentrations in marine rain (resulting in free amino acids = 0.1 M, other primary amines = 4.3×10^{-3} M),[33] and $[NH_4^+]$ = 3 M, its equilibrium concentration in AS aerosol at 95%

227 RH.[34] (Some lab studies have used $[NH_4^+]$ = 6.2 M,[35, 36] its equilibrium concentration at 90% RH.)
228 GAld + OH radical reaction rates were calculated using $k_{OH} = 1.5 \times 10^9$ M^{-1} s^{-1}.[2, 37] Results are
229 summarized in Figure 2. If our rate constants measured here in bulk D_2O are applied to aqueous
230 aerosol particles, Maillard-type reactions between glycolaldehyde and reduced nitrogen
231 compounds would be less important than oxidation by dissolved OH radicals: we estimate that
232 ~20% of aqueous GAld would react at pH 5.5 by Maillard pathways during the day. However, if
233 we set f_{Ald} = 1.0 instead of 0.053 to simulate activation of GAld carbonyl groups at the air-water
234 interface, ~84% of aqueous GAld would react at pH 5.5 by Maillard pathways during the day,
235 mostly by reacting with AS. Setting f_{Ald} = 1.0 instead of 0.053 results in a factor of ~20
236 acceleration of reaction rates in aerosol particles relative to bulk liquid, which is quite modest
237 compared to that observed for glyoxal-AS or glyoxal-amine reactions.[18, 38] Furthermore, fast
238 photolytic radical-initiated oligomerization reactions between aldehyde and amine species in
239 suspended aqueous aerosol particles have also been reported,[39] but are not included in these
240 estimates. We explore GAld reactions in aqueous aerosol in laboratory measurements described
241 in the next section.

242 3.2. Glycolaldehyde reactions in an aerosol-cloud chamber.

243 To test whether GAld reactions with reduced nitrogen species can occur in suspended aqueous
244 aerosol particles on a timescale of minutes to hours (rather than days), a short series of chamber
245 experiments was performed (Table 2). In experiments 2 and 3, aerosol particles were collected on
246 filters for LCMS analysis.
247
248

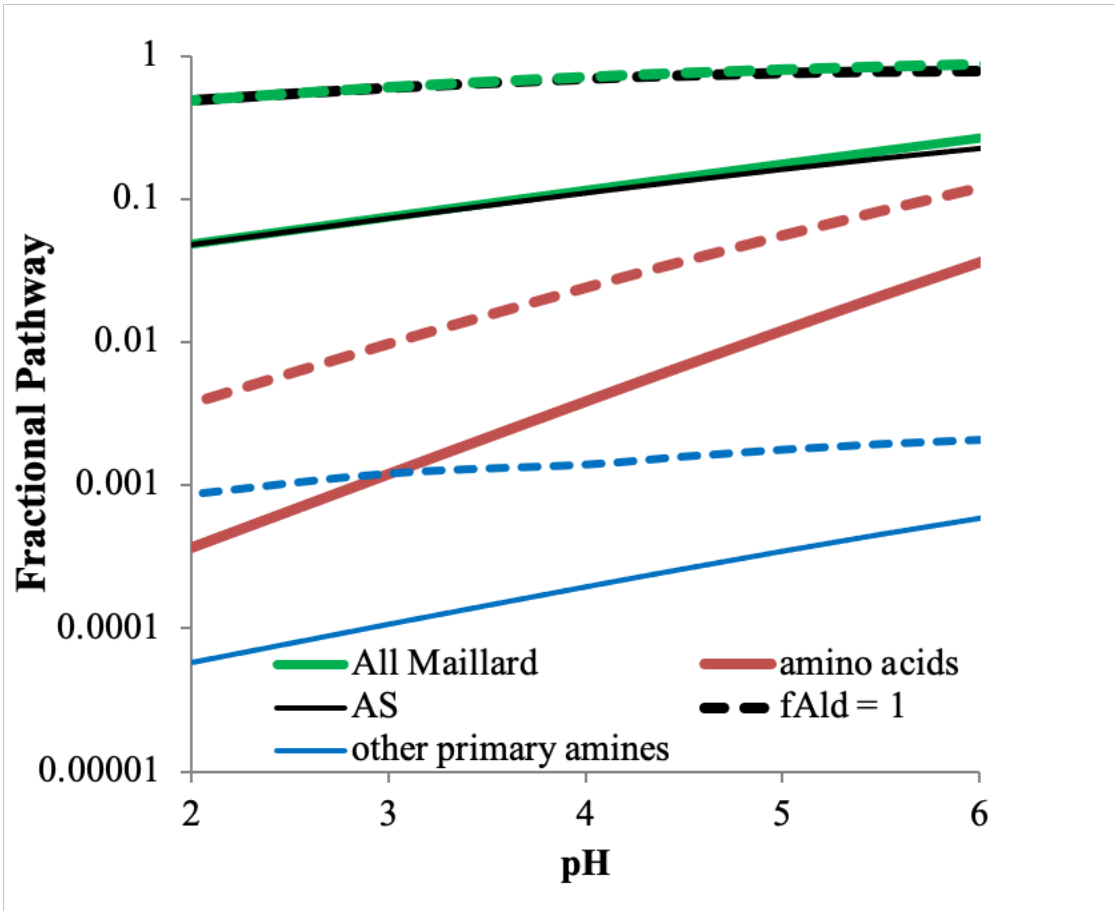

Figure 2: Estimation of fraction of aqueous-phase GAld reacting via various Maillard pathways in daytime marine aerosol as a function of pH, calculated assuming f_{Ald} = 0.053 (solid lines) or f_{Ald} = 1 (dashed lines, $[NH_4^+]$ = 3 M; free amino acids = 0.1 M, all reacting with GAld at the rates measured here in bulk D_2O for glycine; other primary amines = 4.3×10^{-3} M, all reacting with GAld at the rates measured in bulk D_2O for methylamine; and $[OH\ radical]_{aq} = 1 \times 10^{-13}$ M. GAld+AS reaction (black lines), GAld+amino acid reactions (red lines), GAld+amine reactions (blue lines), and sum of all Maillard pathways (green lines, dominated by the GAld + AS reaction) are shown.

In experiment 1 (Figures 3 and S3), diffusion-dried glycine seed aerosol was exposed to water vapor, 1 ppm gas-phase GAld, and cloud processing in the dark. Increasing chamber RH from dry

261 to 50% caused a 18% loss of glycine seed dried particle mass, the introduction of a few trace
262 contaminant gases along with the water vapor (such as acetic acid detected by PTR-MS at *m/z* 43
263 and 61), a large increase in mass-based aerosol scattering efficiency, and a corresponding small
264 increase in the imaginary part of the index of refraction at 450 nm from 0.009 to 0.013. Since 50%
265 RH is well below the deliquescence point for glycine aerosol (~95% RH),[40] it appears that surface
266 reorganization by adsorbed water is responsible for the observed changes in optical properties,
267 which were measured after drying the aerosol. (The PILS-waveguide UV/vis absorbance baseline
268 was unstable for the first 5.5 h of the experiment.) Addition of 1 ppm of GAld gas (detected by
269 PTR-MS at *m/z* 61) did not cause significant changes in seed particle size or optical properties,
270 indicating that GAld uptake into adsorbed water layers is insignificant. However, aerosol
271 deliquescence, followed immediately by fifteen minutes of dark cloud processing, resulted in the
272 loss of 67% of GAld from the gas phase. (Much of this GAld may have gone to the walls – we
273 cannot quantify particle growth during cloud processing because at least 30% of aerosol mass was
274 lost due to wet deposition.) Cloud processing also increased absorbance observed by PILS in wet-
275 sampled aerosol at 365 and 450 nm from 0.0042 to 0.0060, but reduced the imaginary part of the
276 index of refraction at 450 nm in dried aerosol by a factor of 2. The loss of gas-phase GAld
277 corresponding to an increased absorbance in wet-sampled aerosol suggest that at least some GAld
278 was taken up into the aerosol / droplet aqueous phase, where it reacted with glycine to reversibly
279 form brown carbon on a 15-minute timescale. However, this BrC was not stable against drying /
280 evaporation. In the hour after the cloud event, 38% of the GAld taken up from the gas phase was
281 slowly released back to the gas phase as the RH declined to 90%. While much of this release
282 likely came from the chamber walls, some of it likely came from aerosol particles: slow but nearly
283 complete release of GAld from fully dried airborne droplets has been observed in an earlier study,
284 and held as evidence of reversible oligomer formation.[15]

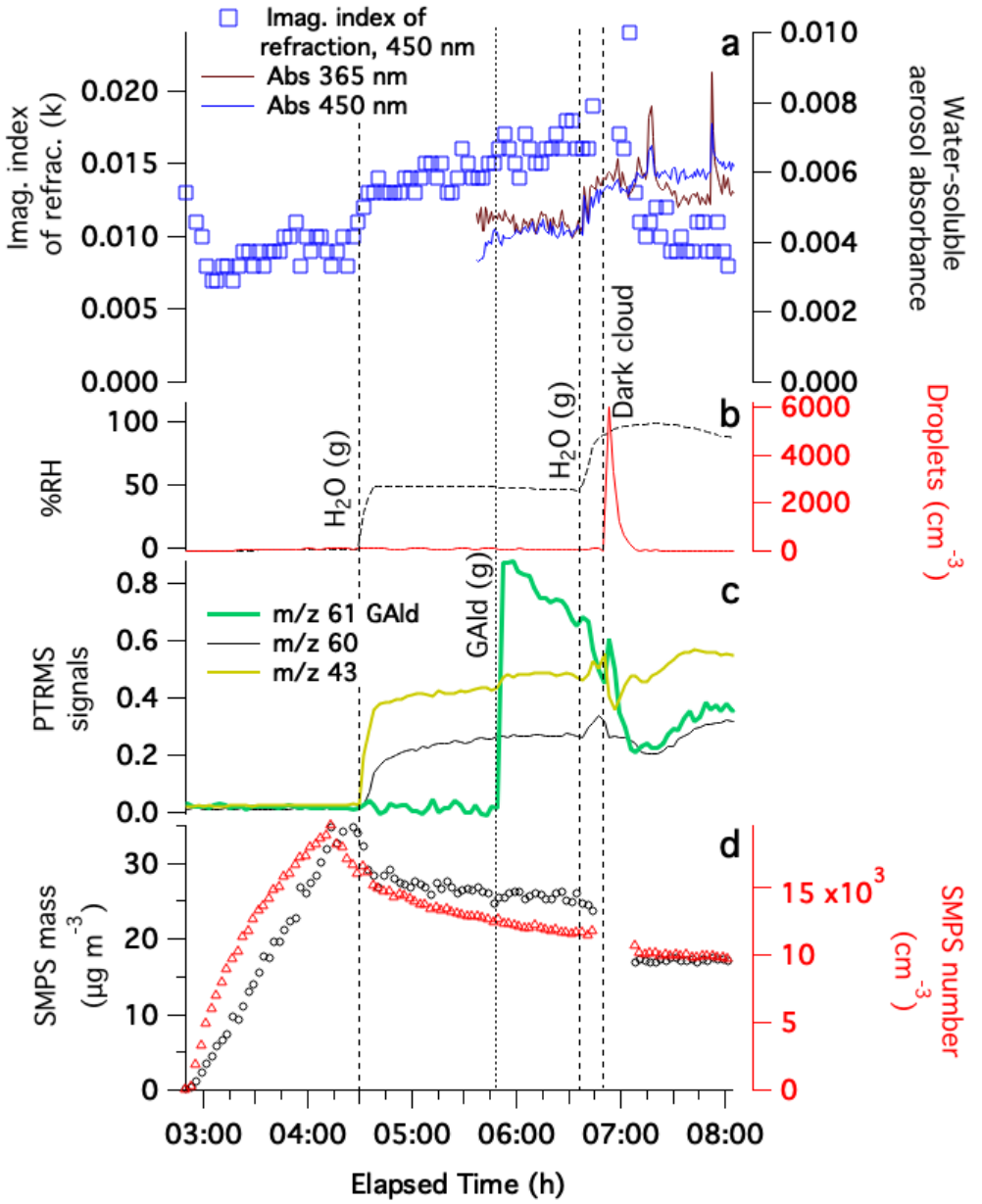

Figure 3: Summary of experiment 1, dried glycine seed particles exposed to GAld gas and cloud processing in the dark. Panel a: time-dependent imaginary part of the index of refraction of dried aerosol extracted from CAPS-ssa data at 450 nm (blue squares), and absorbance of water-soluble aerosol material sampled by PILS at 365 (brown line) and 450 nm (blue line). Panel b: relative humidity (black dotted line), and cloud droplet counts (red line, right axis). Panel c: dilution-corrected PTR-MS signals for *m/z* 43 (acetic acid fragment), 60, and GAld-attributed portion of *m/z* 61. Panel d: dilution-corrected SMPS number density (red triangles, right axis) and mass (black circles). Additions of GAld gas (dots), water vapor addition and cloud events (dashes) are labelled with vertical lines. For CAPS extinction, scattering, and albedo data, see Figure S3.

Experiments 2 and 3 involved mixed AS+GAld seed particles that were either collected without chamber exposure as a control (experiment 3), or exposed to 1 ppm methylamine gas, dark cloud processing, and cloud processing in 60 min. of simulated sunlight before filter collection (experiment 2). Reaction product ions detected in filter extracts by ESI-HRMS in the two experiments are summarized in the next section; optical and physical parameters measured during chamber exposure (experiment 2) are summarized in Figure 4. Seed particles were added without diffusion drying to the chamber at 50-58% RH; under these conditions, aerosol droplets containing AS cannot effloresce but remain aqueous-phase particles. PTR-MS signals at *m/z* 61 indicate that a substantial amount of GAld evaporated from the seed particles (and likely also from the liquid used in the atomization process), reaching a peak of 8.7 ppm in the chamber at the end of the seed particle addition. Even before any further additions to the chamber, absorbance measured in PILS-sampled aerosol reached 0.0055 at 365 nm and 0.0032 at 450 nm, presumably due to brown carbon formed by GAld + AS reactions in the aqueous aerosol particles.

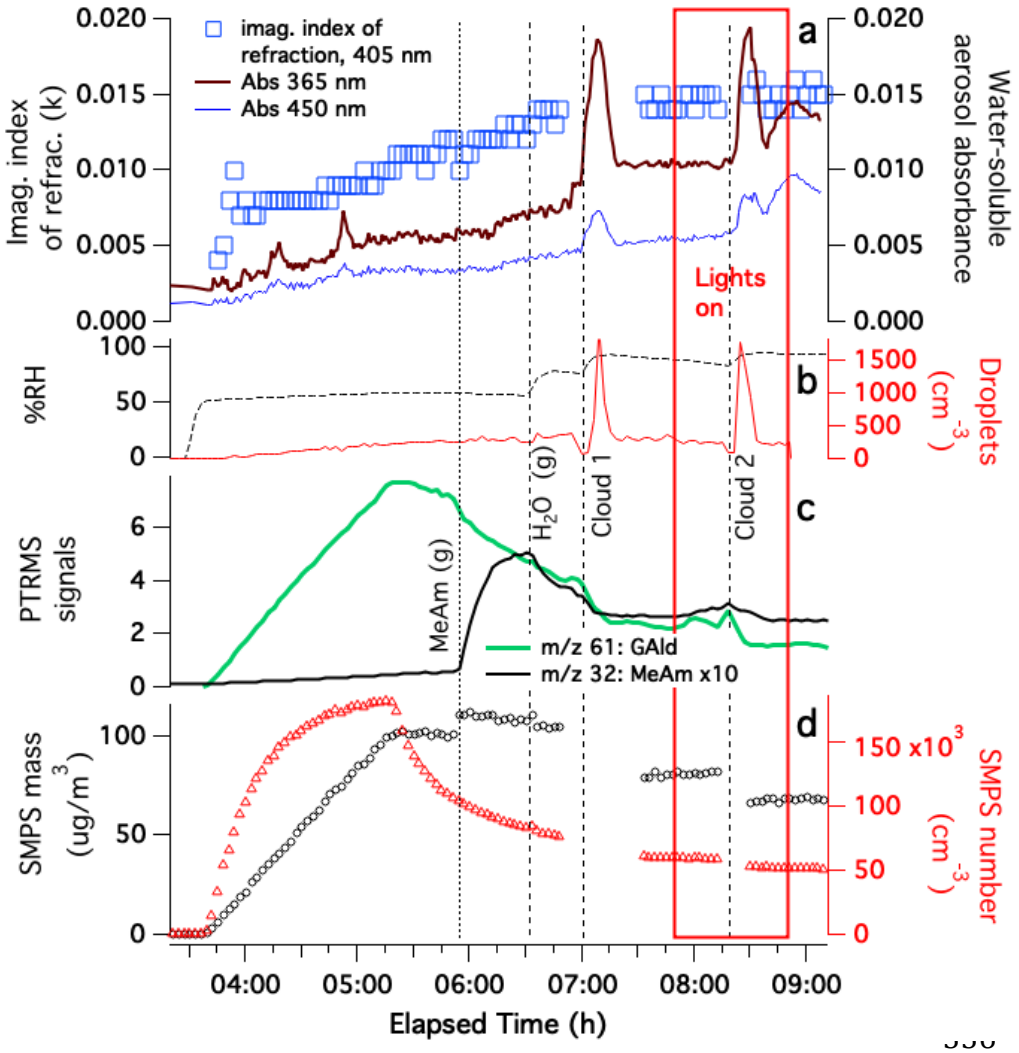

Figure 4: Summary of experiment 2, seed particles generated from 1.8 mM AS / 50 mM GAld solution, added to humidified chamber without drying, and then exposed to methylamine gas, cloud processing, and simulated sunlight. Panel a: Time-dependent imaginary part of the index of refraction of dried aerosol extracted from CAPS-ssa data at 450 nm (blue squares, left axis) and absorbance of water-soluble aerosol material sampled by PILS at 365 (brown line) and 450 nm (blue line). Panel b: relative humidity and cloud droplet counts. Panel c: dilution-corrected PTR-MS signals for methylamine (black line, *m/z* 32 signals multiplied by 10) and GAld-attributed m/z 61 signals (green line). Panel d: dilution-corrected SMPS number density and mass. For CAPS extinction, scattering, and albedo data, see Figure S4.

Addition of 1 ppm methylamine gas to the chamber caused an immediate 9% increase in dried aerosol mass, accelerated the loss rate of GAld from the gas phase (some of which may have gone to the chamber walls), and triggered the start of an upward trend in MAC_{365nm}. These observations suggest that reactive uptake of both methylamine and GAld into the deliquesced aerosol particles occurred, followed by measurable BrC formation. Subsequent dark cloud and sunlit cloud events caused PILS-sampled aerosol absorbance to spike, while irreversibly drawing down ~40% of gas-phase GAld in the chamber, suggesting rapid BrC formation involving GAld. Although aerosol absorbance declines as each cloud dissipates, absorbance after each cloud remains 30-40% higher than it was before the cloud. Unlike in experiment 1, cloud processing (even in simulated sunlight) did not reduce the imaginary part of the index of refraction measured in dried aerosol at 450 nm. These observations indicate that BrC produced in multiphase GAld+AS+methylamine reactions is resistant to drying and also to hydrolysis and photobleaching, as was recently observed in a study conducted on bulk liquid water solutions.[39]

3.3. Aerosol-phase reaction products

Aerosol-phase products detected by LC-ESI-HRMS in GAld+AS seed aerosol extracts before (experiment 3) and after exposure to methylamine gas and both dark and sunlit cloud processing (experiment 2) are shown in Table 3. The four largest peaks detected in GAld+AS seed aerosol (without chamber exposure) are listed in Table 3. Aerosol-phase GAld oligomers are observed, some of which contain nitrogen, indicating that some fraction of GAld reacted with itself or with AS rather than evaporating to the gas phase. We note that that 99.8% of the peak area in the chromatogram of unprocessed GAld + AS aerosol was attributed to molecules built from GAld trimer units (C_6, C_{12}, and C_{24}). Like methylglyoxal, GAld can oligomerize via aldol condensation or acetal formation, forming products by either pathway with identical formulas but different

linkages and structures. While any number of GAld units could oligomerize via acetal formation, we propose that aldol condensation preferentially generates the C_6 intermediate 3-deoxyglucosone (*m/z* 185.0420), which is in equilibrium with a stable cyclic form (Scheme 1), allowing it to accumulate without further aldol additions of GAld monomers. Two 3-deoxyglucosone units can then link via an acetal reaction to form a C_{12} oligomer, bypassing C_8 and C_{10} forms, analogous to sugar chemistry. Thus, the observed preference for products built from C_6 and C_{12} units suggests that GAld, like methylglyoxal,[35] forms oligomers primarily by aldol condensation in aqueous aerosol particles.

377 **Table 3**: Aerosol-phase reaction products detected in glycolaldehyde+AS seed particles before

378 and after exposure to methylamine gas, cloud processing, and simulated sunlight

m/z detected[a] $[M+H]^+$	Peak area rank: Before	Peak area rank: After	Ratio .after . before	Assigned formula of neutral molecule[b]	Δ (ppm)	Possible structure
Ions detected in GAld + AS seed particles before chamber exposure only						
301.1410	1	n/a	0	$C_{13}H_{20}N_2O_6$	-3.5	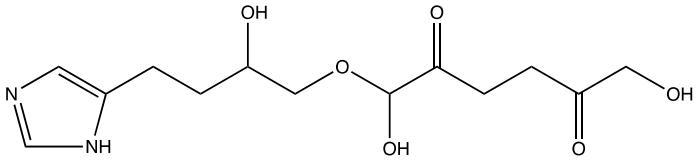
143.0818	2	n/a	0	$C_6H_{10}N_2O_2$	1.9	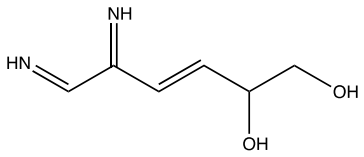
185.0420 $[M+Na]^+$	4	n/a	0	$C_6H_{10}O_5$ GAld trimer: 3-deoxy-glucosone	3.0	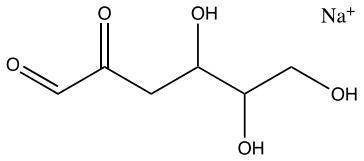
Ions detected in GAld + AS seed particles both before *and* after chamber exposure						
352.2460	11	3	2.3	$C_{16}H_{30}N_7O_2^+$	0.29	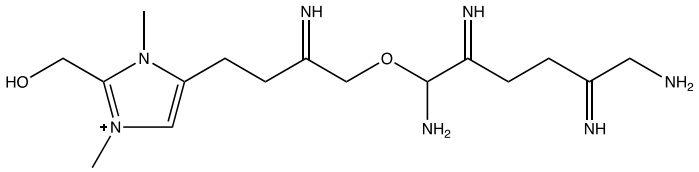
159.0767	14	11	1.2	$C_6H_{10}N_2O_3$	1.6	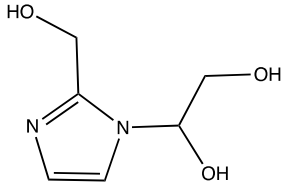
125.0713	9	6	1.1	$C_6H_8N_2O$	1.5	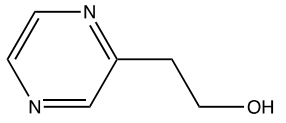 ref [14]
347.0950 $[M+Na]^+$	3	9	0.035[e]	$C_{12}H_{20}O_{10}$	1.1	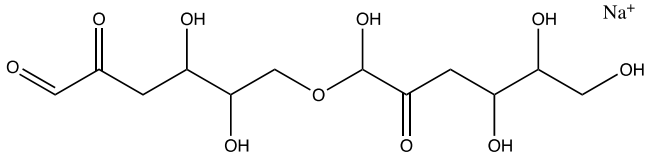

Ions detected in GAld + AS seed particles after chamber exposure only						
196.1082	n/a	1	inf	$C_9H_{13}N_3O_2$	2.0	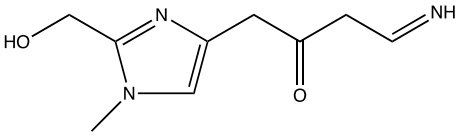
197.0535 $[M+Na]^+$	n/a	2	inf	$C_6H_{10}N_2O_4$	-1.6	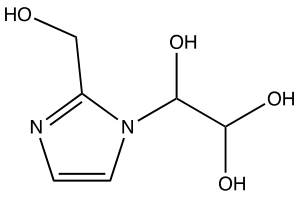
175.0717	n/a	7	inf	$C_6H_{10}N_2O_4$	1.2	
168.0545	n/a	4	inf	$C_4H_9NO_6$	-6.0	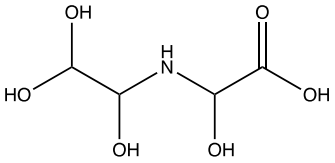
127.5264 $[M+2H]^{2+}$	n/a	5	inf	$C_6H_{11}N_3SO_6$	-0.91	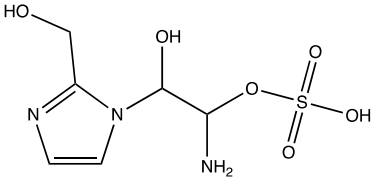
316.1983	n/a	8	inf	$C_{13}H_{25}N_5O_4$	0.51	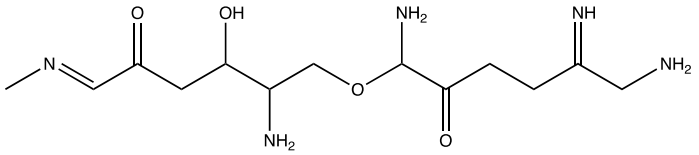
218.1140	n/a	10	inf	$C_8H_{15}N_3O_4$	0.42	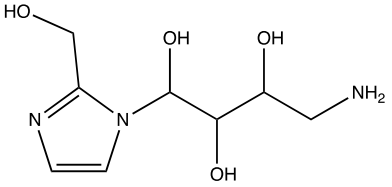

379 Major peaks detected in GAld + AS aerosol by positive ion mode ESI-MS before (experiment
380 3) and after (experiment 2) chamber exposure to methylamine gas, cloud processing, and simulated
381 sunlight. **a**: $[M+H]^+$ ion, unless otherwise stated. **n/a**: peak not detected in given experiment.
382 **inf**: "After / before" ratio infinitely large (division by zero).

383

Scheme 1: Proposed dark mechanism for the preferential formation of C_6 and C_{12} glycolaldehyde oligomers and their reactions with ammonia in aqueous aerosol particles.

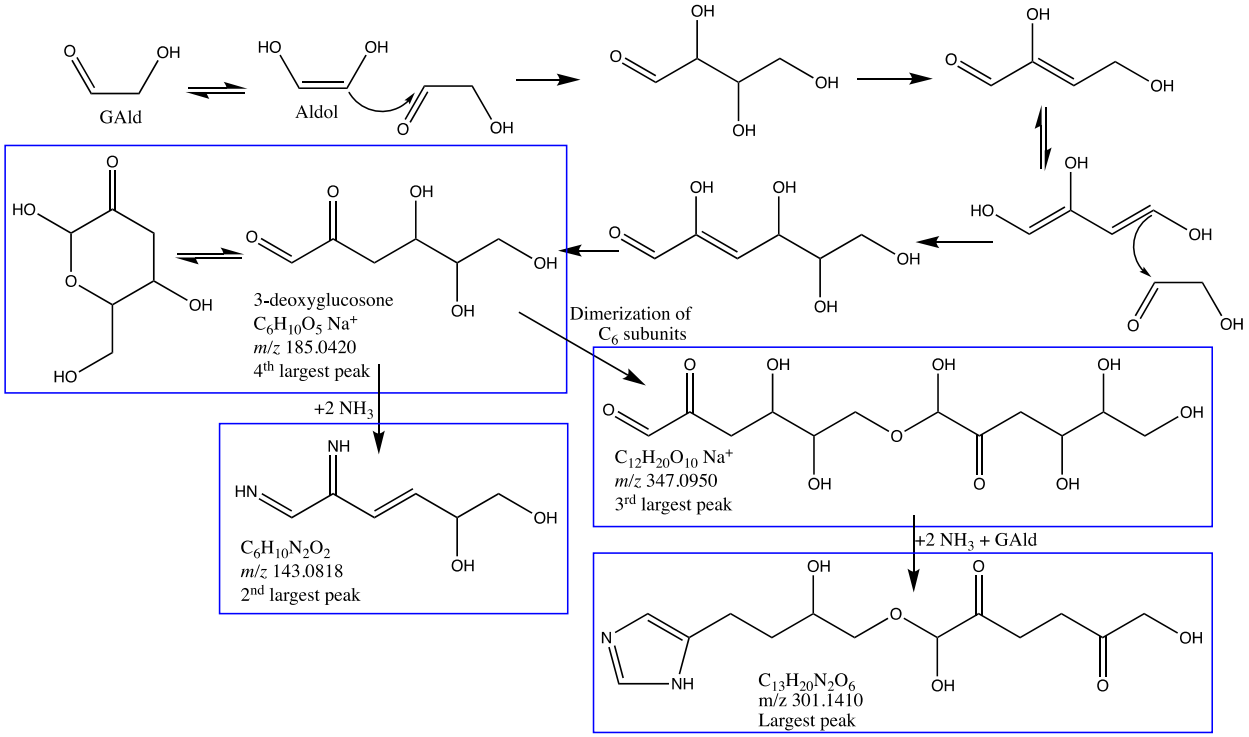

Notes: Blue boxes designate the four largest peaks detected in unprocessed GAld+AS seed aerosol control (experiment 3)

Both 3-deoxyglucosone and its C_{12} "disaccharide" can then be converted by dark reactions with ammonia to diimines and imidazoles, resulting in the two largest peaks detected in unprocessed GAld+AS seed particles: a proposed $C_6H_{10}N_2O_2$ diimine species (*m/z* 143.0818) and a $C_{13}H_{20}N_2O_6$ imidazole derivative (*m/z* 301.1410, 100× larger peak). Imidazole derivatives are typical thermodynamic endpoints for Maillard dark chemistry.[41] In unprocessed GAld+AS seed aerosol (experiment 3), the average number of N atoms / molecule (weighted by peak area)[39] was 2.0, which supports the dominance of diimine and especially imidazole products in terms of concentrations, electrospray ionization efficiencies, or both.

After exposure of GAld+AS seed aerosol to methylamine, cloud processing, and simulated sunlight (experiment 2), the average number of N atoms / molecule detected increased from 2.0 to 2.9. Detected exact masses, proposed formulas, and possible molecular structures are shown in Table 3. Approximately half of this increase in N atoms was due to methylamine incorporation in detected products. The incorporation of ammonia also increased, likely due to the exchange reaction of methylamine with ammonia in the AS-containing aerosol increasing the concentration of dissolved, unprotonated ammonia. The uptake of methylamine into the aerosol particles, seen as an increase in aerosol mass in Figure 4, could also increase the concentration of unprotonated ammonia by raising the pH of the aqueous aerosol phase.

Methylamine exposure, cloud processing, and simulated sunlight reduced the detected abundance of GAld oligomers that do not contain N atoms by 98%, and appear to increase the diversity of product types. N-derivatized C_6 and C_{12} GAld oligomer products are still dominant (making up 68% of the product molecules, weighted by peak area), but a proposed organosulfate imidazole product (*m/z* 127.5264) was also generated during chamber exposure, and the concentration of a pyrazine product identified by Grace *et al.*[14] (*m/z* 125.0713) increased slightly. Four imidazole derivatives formed by nucleophilic attack of the imidazole :NH group on GAld monomers or dimers (analogous to the formation of hydrated N-glyoxal substituted 1H-imidazole in the glyoxal+AS system)[21, 22] are also detected in chamber-exposed GAld+AS aerosol. The average number of conjugated double bonds per detected molecule did not increase in the chamber-exposed aerosol compared to the seed particles, indicating that the increased MAC_{365} observed in PILS-sampled aerosol after cloud processing in the chamber is likely due to other factors. These factors include the greater nitrogen incorporation in organic product molecules (2.9 vs. 2.0 N / molecule detected) and the additional derivatization of imidazoles observed in the chamber-processed aerosol.

4. Discussion & Conclusions

Bulk vs. Aerosol reaction rates. Aerosol particles in experiments 2 – 4 were never dried until collection on filters; the pH of deliquesced AS aerosol has been estimated to be 3.2, with gas-phase ammonia levels in the ambient range having little effect on pH.[42] At this pH, our rate measurements suggest that GAld+AS and GAld+methylamine reactions have similar rate constants ($k \sim 10^{-4}\ M^{-1}\ s^{-1}$). Thermodynamic modeling (E-AIM iii)[34] indicates that in aqueous AS aerosol at 58% RH, ammonium and sulfate ions have a combined mole fraction of 0.4, with ammonium concentrations of ~25 molality (*m)*. Upon methylamine uptake, some ammonium will be exchanged with methylaminium ions, but the total concentration of ammonium and methylaminium ions is likely to remain very high. If the aerosol pH remains at 3.2 after methylamine uptake, the lifetime of any dissolved GAld with respect to amine or ammonia reactions will be ~2 hours. If, however, GAld's dihydrate / aldehyde equilibrium shifts strongly toward the aldehyde at the air-water interface (from $f_{Ald} = 0.053$ to $f_{Ald} = 1$), as has been suggested for other small aldehydes,[24] the lifetime of GAld could become as short as ~7 minutes. This timescale of minutes is more consistent with our aerosol observations: the retention of some GAld in evaporating GAld+AS aerosol droplets (at 58% RH), the detection of GAld oligomers in these particles, and the accelerated uptake of GAld from the gas phase upon introduction of methylamine gas into the chamber (also at 58% RH), all of which took place in minutes.

In contrast, in a more dilute, post-cloud environment at 98% RH, where $[NH_4^+] = 1.1m$, predicted lifetimes for non-hydrated (aldehyde-form) GAld molecules with respect to AS / amine reactions would lengthen to ~2.5 h, and lifetimes in large, activated cloud droplets would be even longer. In these high-RH conditions, bulk phase reaction kinetics, even with a 20-fold acceleration due to surface equilibrium shifts to aldehyde-form GAld (from $f_{Ald} = 0.053$ to $f_{Ald} = 1$), are still an

order of magnitude slower than the spikes in absorbance or the irreversible losses of $GAld_{(g)}$ observed during each 10-minute cloud event. A possible explanation is further surface effects, where GAld preferentially partitions to and reacts at an air-water interface crowded with other surface-active species. Several other aldehyde+AS/amine reaction systems generate surface-active species,[35, 43, 44] including during photolysis.[45]

Atmospheric significance. In the atmosphere at moderate RH, the presence of other substances in aqueous aerosol particles would likely lower effective reactant concentrations,[46] and organic species could lose access to ammonium and aminium salts by "salting out" or by liquid-liquid phase separation of organic and aqueous phases.[47] Both factors would slow down reactions between GAld, AS, and amine species in aqueous aerosol at moderate humidity levels. However, at RH near 100%, Henry's law (rather than other dissolved species) would control GAld concentrations in the droplet, and surface activity could cause surface concentrations of GAld or first-generation GAld+AS/amine products to reach high levels, even though typical atmospheric GAld gas concentrations are significantly lower than the 0.3 – 1 ppm concentrations used in experiments 1 and 4. Additionally, cross reactions between GAld and other aldehydes as they react with AS and amine species, especially those that generate additional surface-active intermediates, may accelerate the incorporation of GAld into BrC oligomers. Cloud processing of GAld in the presence of AS and amine species can therefore be expected to produce brown carbon under atmospheric conditions.

Supporting Information Available

Description of PTR-MS signal corrections for changing water vapor levels, figures describing deconvolution of acetic acid and GAld signals at *m/z* 61, figures summarizing chamber experiments 1, 2, and 4 including extinction, scattering, and single-scattering albedo measurements

at 450 nm, and a listing of all peaks detected by ESI-HRMS in the aerosol extracts. Raw data from aerosol – cloud chamber experiments is available in a data repository.[48]

Acknowledgments

This work was supported by NSF grants AGS-1129002 and AGS-1826593. The CESAM chamber and associated control experiments were part of a project that has received funding from the European Union's Horizon 2020 research and innovation program under grant agreement No. 730997. CNRS-INSU is gratefully acknowledged for supporting CESAM as an open facility through the National Instrument label, as well as the AERIS data center (https://www.aeris-data.fr/) for hosting, curating, and distributing CESAM chamber data via EUROCHAMP-2020 databases. The LC-ESI-HRMS measurements were performed on project award 10.46936/sthm.proj.2015.48884/60005735 at the Environmental Molecular Sciences Laboratory, a DOE Office of Science User Facility sponsored by the Biological and Environmental Research program under Contract No. DE-AC05-76RL01830.

References

(1) Spaulding, R. S.; Schade, G. W.; Goldstein, A. H.; Charles, M. J. Characterization of secondary atmospheric photooxidation products: evidence for biogenic and anthropogenic sources. *Journal of Geophysical Research, [Atmospheres]* **2003**, *108* (D8), 4247. DOI: 10.1029/2002jd002478.

(2) Perri, M. J.; Seitzinger, S.; Turpin, B. J. Secondary organic aerosol production from aqueous photooxidation of glycolaldehyde: Laboratory experiments. *Atmos. Environ.* **2009**, *43* (8), 1487-1497. DOI: 10.1016/j.atmosenv.2008.11.037.

(3) Butkovskaya, N. I.; Pouvesle, N.; Kukui, A.; Le Bras, G. Mechanism of the OH-Initiated Oxidation of Glycolaldehyde over the Temperature Range 233−296 K. *The Journal of Physical Chemistry A* **2006**, *110* (50), 13492-13499. DOI: 10.1021/jp064993k.

(4) Magneron, I.; Mellouki, A.; Le Bras, G.; Moortgat, G. K.; Horowitz, A.; Wirtz, K. Photolysis and OH-Initiated Oxidation of Glycolaldehyde under Atmospheric Conditions. *The Journal of Physical Chemistry A* **2005**, *109* (20), 4552-4561. DOI: 10.1021/jp044346y.

(5) Bacher, C.; Tyndall, G. S.; Orlando, J. J. The atmospheric chemistry of glycolaldehyde. *J. Atmos. Chem.* **2001**, *39*, 171-189. DOI: 10.1023/A:1010689706869.

(6) Matsunaga, S.; Mochida, M.; Kawamura, K. Variation on the atmospheric concentrations of biogenic carbonyl compounds and their removal processes in the northern forest at Moshiri, Hokkaido Island in Japan. *J. Geophys. Res.* **2004**, *109*, D04302.
(7) van Pinxteren, D.; Plewka, A.; Hofmann, D.; Muller, K.; Kramberger, H.; Svrcina, B.; Bachmann, K.; Jaeschke, W.; Mertes, S.; Collett Jr., J. L.; et al. Schmucke hill cap cloud and valley stations aerosol characterisation during FEBUKO (II): organic compounds. *Atmos. Environ.* **2005**, *39*, 4305-4320. DOI: 10.1016/j.atmosenv.2005.02.014.
(8) Müller, K.; van Pinxteren, D.; Plewka, A.; Svrcina, B.; Kramberger, H.; Hofmann, D.; Bächmann, K.; Herrmann, H. Aerosol characterisation at the FEBUKO upwind station Goldlauter (II): Detailed organic chemical characterisation. *Atmos. Environ.* **2005**, *39* (23), 4219-4231. DOI: 10.1016/j.atmosenv.2005.02.008.
(9) Matsumoto, K.; Kawai, S.; Igawa, M. Dominant factors controlling concentrations of aldehydes in rain, fog, dew water, and in the gas phase. *Atmos. Environ.* **2005**, *39*, 7321-7329.
(10) Gkatzelis, G. I.; Papanastasiou, D. K.; Karydis, V. A.; Hohaus, T.; Liu, Y.; Schmitt, S. H.; Schlag, P.; Fuchs, H.; Novelli, A.; Chen, Q.; et al. Uptake of water-soluble gas-phase oxidation products drives organic particulate pollution in Beijing. *Geophys. Res. Lett.* **2021**, *48* (8), e2020GL091351, https://doi.org/10.1029/2020GL091351. DOI: 10.1029/2020GL091351 (acccessed 2021/04/08).
(11) Perri, M. J.; Lim, Y.-B.; Seitzinger, S. P.; Turpin, B. J. Organosulfates from glycolaldehyde in aqueous aerosols and clouds: Laboratory studies. *Atmos. Environ.* **2010**, *44* (21-22), 2658-2664, 10.1016/j.atmosenv.2010.03.031. DOI: 10.1016/j.atmosenv.2010.03.031.
(12) Nguyen, T. B.; Coggon, M. M.; Flagan, R. C.; Seinfeld, J. H. Reactive Uptake and Photo-Fenton Oxidation of Glycolaldehyde in Aerosol Liquid Water [Erratum to document cited in CA158:609086]. *Environ. Sci. Technol.* **2013**, *47* (17), 10093, 10.1021/es403622y. DOI: 10.1021/es403622y.
(13) Powelson, M. H.; Espelien, B. M.; Hawkins, L. N.; Galloway, M. M.; De Haan, D. O. Brown carbon formation by aqueous-phase aldehyde reactions with amines and ammonium sulfate. *Environ Sci Technol* **2014**, *48* (2), 985-993. DOI: 10.1021/es4038325.
(14) Grace, D. N.; Sharp, J. R.; Holappa, R. E.; Lugos, E. N.; Sebold, M. B.; Griffith, D. R.; Hendrickson, H. P.; Galloway, M. M. Heterocyclic Product Formation in Aqueous Brown Carbon Systems. *ACS Earth and Space Chemistry* **2019**, *3* (11), 2472-2481. DOI: 10.1021/acsearthspacechem.9b00235.
(15) Galloway, M. M.; Powelson, M. H.; Sedehi, N.; Wood, S. E.; Millage, K. D.; Kononenko, J. A.; Rynaski, A. D.; De Haan, D. O. Secondary organic aerosol formation during evaporation of droplets containing atmospheric aldehydes, amines, and ammonium sulfate. *Environ Sci Technol* **2014**, *48*, 14417-14425. DOI: 10.1021/es5044479.
(16) Stangl, C. M.; Johnston, M. A.-O. Aqueous Reaction of Dicarbonyls with Ammonia as a Potential Source of Organic Nitrogen in Airborne Nanoparticles. (1520-5215 (Electronic)). From 2017 May 18.
(17) Kua, J.; Galloway, M. M.; Millage, K. D.; Avila, J. E.; De Haan, D. O. Glycolaldehyde Monomer and Oligomer Equilibria in Aqueous Solution: Comparing Computational Chemistry and NMR Data. *The Journal of Physical Chemistry A* **2013**, *117* (14), 2997-3008. DOI: 10.1021/jp312202j.
(18) De Haan, D. O.; Corrigan, A. L.; Smith, K. W.; Stroik, D. R.; Turley, J. T.; Lee, F. E.; Tolbert, M. A.; Jimenez, J. L.; Cordova, K. E.; Ferrell, G. R. Secondary organic aerosol-forming

reactions of glyoxal with amino acids. *Environ. Sci. Technol.* **2009**, *43* (8), 2818-2824. DOI: 10.1021/es803534f.
(19) De Haan, D. O.; Tolbert, M. A.; Jimenez, J. L. Atmospheric condensed-phase reactions of glyoxal with methylamine. *Geophys. Res. Lett.* **2009**, *36*, L11819. DOI: 10.1029/2009gl037441.
(20) Noziere, B.; Dziedzic, P.; Cordova, A. Products and kinetics of the liquid-phase reaction of glyoxal catalyzed by ammonium ions (NH_4^+). *J. Phys. Chem.* **2009**, *113* (1), 231-237. DOI: 10.1021/jp8078293.
(21) Yu, G.; Bayer, A. R.; Galloway, M. M.; Korshavn, K. J.; Fry, C. G.; Keutsch, F. N. Glyoxal in aqueous ammonium sulfate solutions: products, kinetics, and hydration effects. *Environ. Sci. Technol.* **2011**, *45*, 6336-6342. DOI: 10.1021/es200989n.
(22) Kampf, C. J.; Jakob, R.; Hoffmann, T. Identification and characterization of aging products in the glyoxal/ammonium sulfate system -- implications for light-absorbing material in atmospheric aerosols. *Atmos. Chem. Phys.* **2012**, *12*, 6323-6333. DOI: 10.5194/acp-12-6323-2012.
(23) Noziere, B.; Cordova, A. A kinetic and mechanistic study of the amino acid catalyzed aldol condensation of acetaldehyde in aqueous and salt solutions. *J. Phys. Chem.* **2008**, *112* (13), 2827-2837. DOI: 10.1021/jp7096845.
(24) Sedehi, N.; Takano, H.; Blasic, V. A.; Sullivan, K. A.; De Haan, D. O. Temperature- and pH-dependent aqueous-phase kinetics of the reactions of glyoxal and methylglyoxal with atmospheric amines and ammonium sulfate. *Atmos. Environ.* **2013**, *77*, 656-663. DOI: 10.1016/j.atmosenv.2013.05.070.
(25) Glushonok, G. K.; Glushonok, T. G.; Shadyro, O. I. Kinetics of equilibrium attainment between molecular glycolaldehyde structures in an aqueous solution. *Kinetics and Catalysis* **2000**, *41* (5), 620-624. DOI: 10.1007/BF02754560.
(26) Wang, J.; Doussin, J. F.; Perrier, S.; Perraudin, E.; Katrib, Y.; Pangui, E.; Picquet-Varrault, B. Design of a new multi-phase experimental simulation chamber for atmospheric photosmog, aerosol and cloud chemistry research. *Atmos. Meas. Tech.* **2011**, *4*, 2465-2494. DOI: 10.5194/amt-4-2465-2011.
(27) De Haan, D. O.; Tapavicza, E.; Riva, M.; Cui, T.; Surratt, J.; Smith, A. C.; Jordan, M.-C.; Nilakantan, S.; Almodovar, M.; Stewart, T. N.; et al. Nitrogen-containing, light-absorbing oligomers produced in aerosol particles exposed to methylglyoxal, photolysis, and cloud cycling. *Environ. Sci. Technol.* **2018**, *52* (7), 4061-4071. DOI: 10.1021/acs.est.7b06105.
(28) Onasch, T. B.; Massoli, P.; Kebabian, P. L.; Hills, F. B.; Bacon, F. W.; Freedman, A. Single scattering albedo monitor for airborne particulates. *Aerosol Sci. Technol.* **2015**, *49* (4), 267-279. DOI: 10.1080/02786826.2015.1022248.
(29) Lin, P.; Fleming, L. T.; Nizkorodov, S. A.; Laskin, J.; Laskin, A. Comprehensive Molecular Characterization of Atmospheric Brown Carbon by High Resolution Mass Spectrometry with Electrospray and Atmospheric Pressure Photoionization. *Anal. Chem.* **2018**, *90* (21), 12493-12502. DOI: 10.1021/acs.analchem.8b02177.
(30) Lin, P.; Laskin, J.; Nizkorodov, S. A.; Laskin, A. Revealing Brown Carbon Chromophores Produced in Reactions of Methylglyoxal with Ammonium Sulfate. *Environ Sci Technol* **2015**, *49* (24), 14257-14266. DOI: 10.1021/acs.est.5b03608.
(31) Noziere, B.; Dziedzic, P.; Cordova, A. Inorganic ammonium salts and carbonate salts are efficient catalysts for aldol condensation in atmospheric aerosols. *Phys. Chem. Chem. Phys.* **2010**, *12* (15), 3864-3872, 10.1039/b924443c. DOI: 10.1039/b924443c.

(32) Ervens, B.; George, C.; Williams, J. E.; Buxton, G. V.; Salmon, G. A.; Bydder, M.; Wilkinson, F.; Dentener, F.; Mirabel, P.; Wolke, R.; et al. CAPRAM 2.4 (MODAC mechanism): An extended and condensed tropospheric aqueous phase mechanism and its application. *Journal of Geophysical Research: Atmospheres* **2003**, *108* (D14), https://doi.org/10.1029/2002JD002202. DOI: 10.1029/2002JD002202 (acccessed 2022/01/17).
(33) Mopper, K.; Zika, R. G. Free amino acids in marine rains: evidence for oxidation and potential role in nitrogen cycling. *Nature* **1987**, *325*, 246-249. DOI: doi.org/10.1038/325246a0.
(34) Clegg, S. L.; Brimblecombe, P.; Wexler, A. S. Thermodynamic Model of the System H+−NH4+−Na+−SO42-−NO3-−Cl-−H2O at 298.15 K. *The Journal of Physical Chemistry A* **1998**, *102* (12), 2155-2171. DOI: 10.1021/jp973043j.
(35) Sareen, N.; Schwier, A. N.; Shapiro, E. L.; Mitroo, D.; McNeill, V. F. Secondary organic material formed by methylglyoxal in aqueous aerosol mimics. *Atmos. Chem. Phys.* **2010**, *10*, 997-1016. DOI: 10.5194/acp-10-997-2010.
(36) Shapiro, E. L.; Szprengiel, J.; Sareen, N.; Jen, C. N.; Giordano, M. R.; McNeill, V. F. Light-absorbing secondary organic material formed by glyoxal in aqueous aerosol mimics. *Atmos. Chem. Phys.* **2009**, *9*, 2289-2300. DOI: 10.5194/acp-9-2289-2009.
(37) Warneck, P. In-cloud chemistry opens pathway to the formation of oxalic acid in the marine atmosphere. *Atmos. Environ.* **2003**, *37* (17), 2423-2427. DOI: 10.1016/S1352-2310(03)00136-5.
(38) Lee, A. K. Y.; Zhao, R.; Li, R.; Liggio, J.; Li, S.-M.; Abbatt, J. P. D. Formation of light absorbing organo-nitrogen species from evaporation of droplets containing glyoxal and ammonium sulfate. *Environ Sci Technol* **2013**, *47* (22), 12819-12826. DOI: 10.1021/es402687w.
(39) Jimenez, N. G.; Sharp, K. D.; Gramyk, T.; Ugland, D. Z.; Tran, M.-K.; Rojas, A.; Rafla, M. A.; Stewart, D.; Galloway, M. M.; Lin, P.; et al. Radical-Initiated Brown Carbon Formation in Sunlit Carbonyl–Amine–Ammonium Sulfate Mixtures and Aqueous Aerosol Particles. *ACS Earth and Space Chemistry* **2022**. DOI: 10.1021/acsearthspacechem.1c00395.
(40) Chan, M. N.; Choi, M. Y.; Ng, N. L.; Chan, C. K. Hygroscopicity of water-soluble organic compounds in atmospheric aerosols: amino acids and biomass derived organic species. *Environ. Sci. Technol.* **2005**, *39* (6), 1555-1562. DOI: 10.1021/es049584l.
(41) Kua, J.; Krizner, H. E.; De Haan, D. O. Thermodynamics and kinetics of imidazole formation from glyoxal and methylamine: a computational study. *J. Phys. Chem.* **2011**, *115* (9), 1667-1675. DOI: 10.1021/jp111527x.
(42) Guo, H.; Weber, R. J.; Nenes, A. High levels of ammonia do not raise fine particle pH sufficiently to yield nitrogen oxide-dominated sulfate production. *Sci Rep* **2017**, *7* (1), 12109-12109. DOI: 10.1038/s41598-017-11704-0 PubMed.
(43) Li, Z.; Schwier, A. N.; Sareen, N.; McNeill, V. F. Reactive processing of formaldehyde and acetaldehyde in aqueous aerosol mimics: surface tension depression and secondary organic products. *Atmos. Chem. Phys.* **2011**, *11* (22), 11617-11629. DOI: 10.5194/acp-11-11617-2011.
(44) Sareen, N.; Schwier, A. N.; Lathem, T. L.; Nenes, A.; McNeill, V. F. Surfactants from the gas phase may promote cloud droplet formation. *Proc. Natl. Acad. Sci. (USA)* **2013**, *110* (8), 2723-2728. DOI: 10.1073/pnas.1204838110.
(45) Beier, T.; Cotter, E. R.; Galloway, M. M.; Woo, J. L. In Situ Surface Tension Measurements of Hanging Droplet Methylglyoxal/Ammonium Sulfate Aerosol Mimics under

638 Photooxidative Conditions. *ACS Earth and Space Chemistry* **2019**, *3* (7), 1208-1215. DOI:
639 10.1021/acsearthspacechem.9b00123.
640 (46) Drozd, G. T.; McNeill, V. F. Organic matrix effects on the formation of light-absorbing
641 compounds from [small alpha]-dicarbonyls in aqueous salt solution. *Environmental*
642 *Science: Processes & Impacts* **2014**, *16* (4), 741-747, 10.1039/C3EM00579H. DOI:
643 10.1039/C3EM00579H.
644 (47) Bertram, A. K.; Martin, S. T.; Hanna, S. J.; Smith, M. L.; Bodsworth, A.; Chen, Q.; Kuwata,
645 M.; Liu, A.; You, Y.; Zorn, S. R. Predicting the relative humidities of liquid-liquid phase
646 separation, efflorescence, and deliquescence of mixed particles of ammonium sulfate,
647 organic material, and water using the organic-to-sulfate mass ratio of the particle and the
648 oxygen-to-carbon elemental ratio of the organic component. *Atmos. Chem. Phys.* **2011**, *11*,
649 10995-11006. DOI: 10.5194/acp-11-10995-2011.
650 (48) De Haan, D. O.; Rodriguez, A. A.; Rafla, M. A.; Welsh, H. G.; Pennington, E. A.; Casar, J. R.;
651 Hawkins, L. N.; Jimenez, N. G.; de Loera, A.; Stewart, D.; et al. Kinetics, products, and
652 brown carbon formation by aqueous-phase reactions of glycolaldehyde with
653 atmospheric amines and ammonium sulfate (Raw data). In *Chemistry and Biochemistry:*
654 *Faculty Scholarship*, University of San Diego: 2022; Vol. 42. DOI: 10.22371/02.2022.009
655

656

657

658 TOC Graphic:

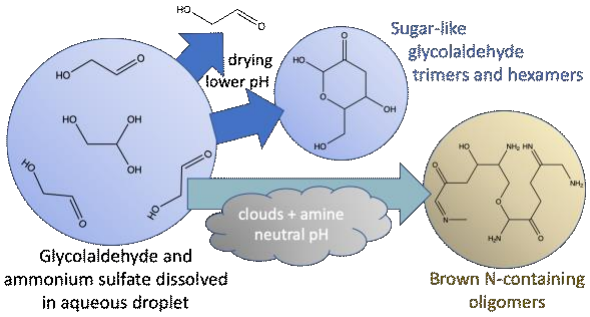

659